Semiconductor Science and Technology

PAPER

Combined STEM-EDS tomography of nanowire structures

To cite this article: Hugo Bender *et al* 2019 *Semicond. Sci. Technol.* **34** 114002

IOP Publishing Semiconductor Science and Technology
Semicond. Sci. Technol. 34 (2019) 114002 (12pp) https://doi.org/10.1088/1361-6641/ab4840

Combined STEM-EDS tomography of nanowire structures

Hugo Bender[1], Olivier Richard[1], Paromita Kundu[1], Paola Favia[1], Zhichao Zhong[2], Willem Jan Palenstijn[2], Kees Joost Batenburg[2], Maarten Wirix[3], Holger Kohr[3] and Remco Schoenmakers[3]

[1] Imec, Kapeldreef 75, B-3001 Leuven, Belgium
[2] Centrum Wiskunde & Informatica, Amsterdam, The Netherlands
[3] Thermo Fisher Scientific, Achtseweg Noord 5, 5600 KA Eindhoven, The Netherlands

E-mail: hugo.bender@imec.be

Received 1 July 2019, revised 5 September 2019
Accepted for publication 26 September 2019
Published 17 October 2019

Abstract

The 3D spatial resolution, the material contrast and the evolution of the noise are analyzed in the reconstructed volume of a combined scanning transmission electron microscopy (HAADF-STEM) and energy dispersive x-ray spectroscopy (EDS) tomography experiment. Standard simultaneous iterative reconstruction technique and HAADF-EDS bimodal tomographic reconstruction are considered for the $+/-90^{\circ}$ tomography series of a pillar shaped sample embedding a full nanowire device. With a high number of iterations, a spatial resolution for both HAADF and EDS down to 5 nanometer can be reached for this volume. Best material's contrast and minimum noise are obtained for medium number of iterations. Improvement of the signal-to-noise and contrast can be obtained by filtering the EDS data while the spatial resolution is not impacted. A fast and reliable preparation methodology for rectangularly shaped pillar samples for tomography analysis is discussed.

Supplementary material for this article is available online

Keywords: STEM tomography, EDS tomography, HEBT tomography reconstruction, nanowire device, pillar tomography sample

(Some figures may appear in colour only in the online journal)

Introduction

For the future scaling of semiconductor technology, 3D nanowire devices with gate-all-around are heavily studied [1]. As the nanowire dimensions are below 5–10 nm, 3D structural and chemical analysis with nanometer scale resolution is needed for process development and control. Scanning transmission electron microscopy (STEM) tomography for structural analysis of semiconductor devices has been considered already for quite some time [2–4]. The possibilities for 3D energy dispersive x-ray spectroscopy (EDS or EDX) tomography were first discussed by Möbus *et al* in 2003 [5]. To reach acceptable signal-to-noise (S/N) levels, long acquisition times and limited number of tilt steps were applied so that only poor spatial resolution could be reached. With the recent development of high-performance EDS detectors, these limitations are strongly reduced so that EDS-tomography is nowadays a feasible option for 3D chemical analysis [6–11].

The tomography experiment yields a series of 2D projection images, in case of EDS generally called elemental maps, acquired over a range of tilt angles. Many methods are proposed in literature for the 3D reconstruction of the original 3D sample volume [2, 12, 13]. Widely used algorithms are weighted backprojection (WBP) and the simultaneous iterative reconstruction technique (SIRT) [14]. The latter results in a strong reduction of the noise in the reconstructions compared to the faster WBP [2]. To minimize the artefacts induced by the discrete number of tilt steps and by the 'missing wedge' due to the geometrically limited tilt range, methods that introduce additional knowledge in the reconstruction procedure are proposed as e.g. discrete algebraic reconstruction tomography, compressed sensing tomography

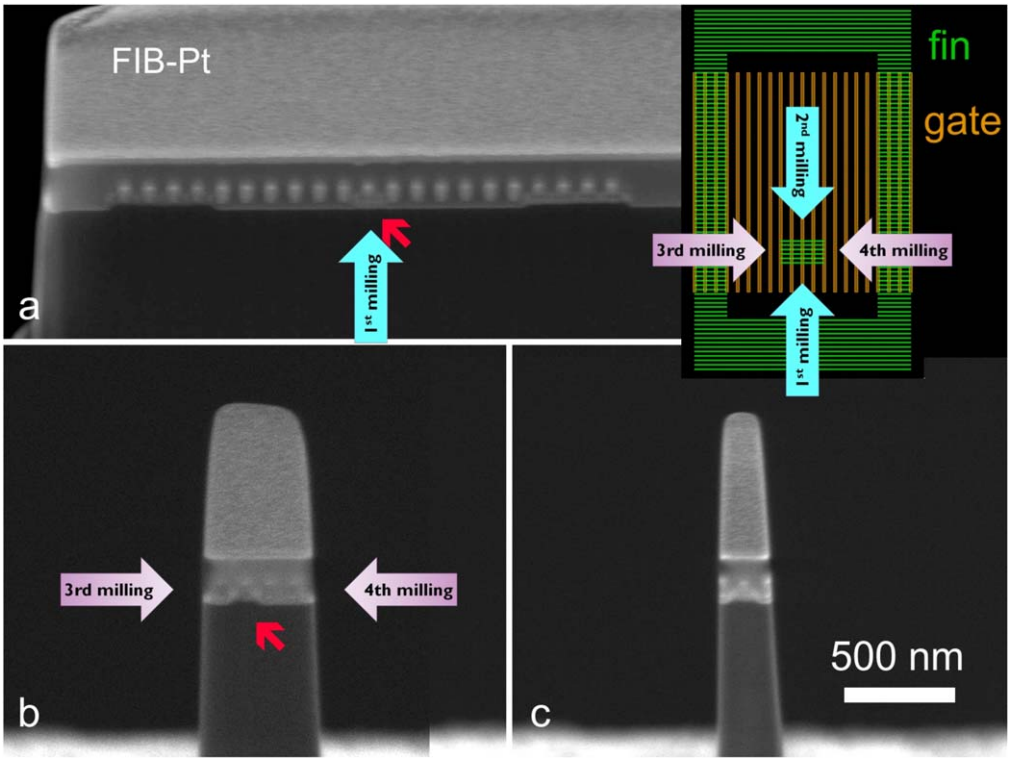

Figure 1. Rectangular pillar preparation for STEM-EDS tomography: (a) after mounting a standard FIB-chunk on top of a W wire (not shown) a standard planar lamella is made by milling in the first and second directions (blue arrows on the top view layout) to the region of interest. The gates run in the viewing direction and are easily recognized on the SEM image. The fin starts to appear at the red arrow. (b) Next, while monitoring the milling progress towards the gates with the SEM image, milling left to right (3rd milling) and right to left (4th milling) is performed resulting in finally a rectangular pillar (c) with the selected fins and gate well positioned in the specimen volume.

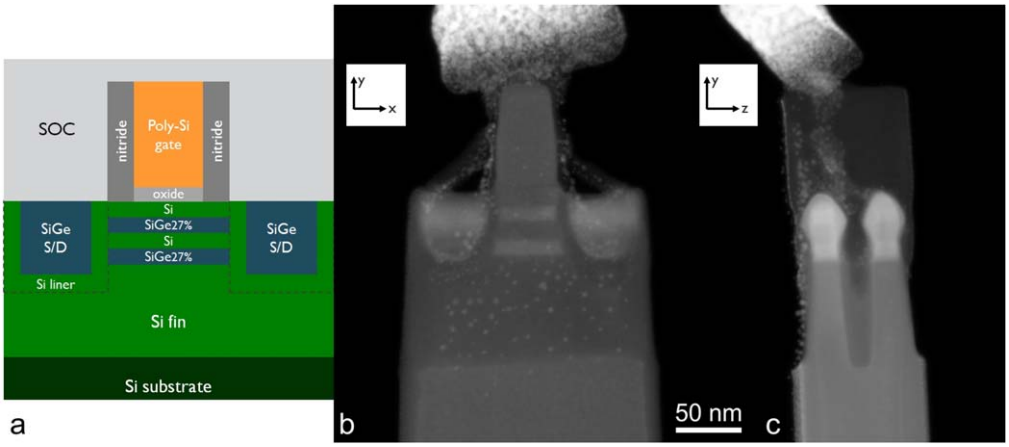

Figure 2. Schematic of the investigated structure (a) and HAADF-STEM images of the pillar sample oriented nearly along the $<110>_{Si}$ directions, i.e. view along the gate (b) and along the fins (c).

or total variation minimization. Combining several methods sequentially [12] or with a multi-channel fusion algorithm [15], is proposed to take advantage of the benefits of each method on its own.

For combined HAADF-EDS tomography, reconstruction with the common back-projection methods can be applied to the datasets of STEM and each element involved separately while using for all data the alignment of the tilt series based on the STEM images. Merging the input of the HAADF reconstruction to the EDS tomography was first proposed by Saghi *et al* [16] to reduce the backprojection artefacts. Recently, a new tomographic reconstruction method that combines the STEM and EDS datasets in a simultaneous reconstruction, 'HAADF-EDS bimodal tomographic reconstruction—HEBT' is presented [17]. It was shown that for phantom objects and Au–Ag particles the method leads to suppressed noise and enhanced contrast. Spatial resolution was not investigated in that work.

To obtain full 3D resolution, acquisition over a 180° tilt range using pillar shaped specimens is mandatory. Such

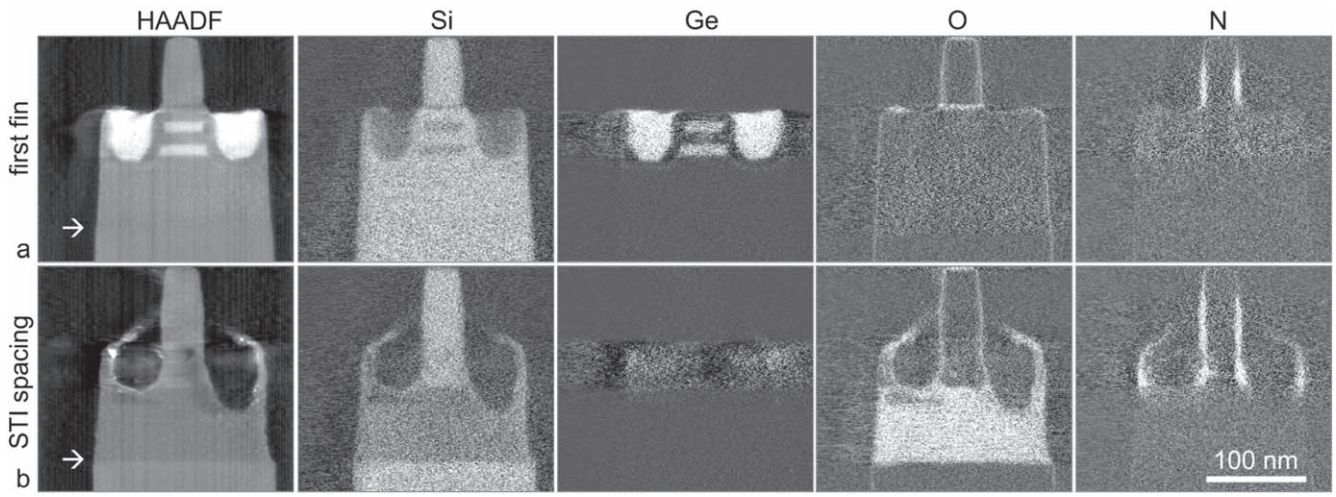

Figure 3. *xy*-slices through (a) the first fin and (b) in the STI oxide spacing between the fins as obtained with 40 SIRT iterations for HAADF, Si K, Ge L, O K and N K. The interfaces substrate/bulk fin and substrate/STI oxide are marked with the arrows on the HAADF slices.

samples can be prepared by focused ion beam (FIB). A pillar configuration also avoids any shadowing effects of the sample holder for the x-rays towards the EDS detector [10, 18].

The spatial resolution possible with electron tomography was first discussed by Crowther *et al* [19]. The expression derived in that work did not consider the effect of iterative reconstructions. Mezerji *et al* [20] showed experimentally that for HAADF-STEM tomography with an approximately $+/-70^\circ$ tilt range applied to 5–30 nm nanoparticle samples, a two times better spatial resolution can be obtained than predicted by the Crowther expression. With the simultaneous iterative reconstruction tomography (SIRT) method they obtained sub-2 nm resolution when at least 20 iterations were applied. A worse resolution was obtained along the optical axis due to the missing wedge effect and for increasing particle size. On the other hand, the noise increases for larger number of iterations. Similar spatial resolution is also reported for semiconductor structures in few hundred nanometer thick specimens [2] and for Sn-rich quantum dots embedded in a Si matrix [21]. Using the prior knowledge of the discrete nature of the atoms combined with statistical parameter estimation, atomic resolution can be obtained for HAADF-STEM tomography of small particles [22]. Spatial resolution for spectroscopic tomography is not extensively discussed yet. Möbus *et al* [5] speculated that resolution around 1 nm should be reachable with advanced equipment, but an experimental study on EDS spatial resolution is not available.

In this work, the 3D spatial resolution, the contrast between different materials, and the noise in the reconstruction are investigated for combined STEM-EDS tomography obtained with a $+/-90^\circ$ tilt range and applied to an advanced 3D nanodevice structure comprising light (O, N) and medium heavy (Ge) elements. The focus is on application with the recent HEBT [17] method which results in a full correlation between the HAADF-STEM and EDS reconstructed volumes. Rectangular-shaped pillar specimens are prepared enclosing the source/drain and gate on top of several Si/SiGe multilayer fin structures. The SIRT [14] tomographic reconstruction method as applied to the STEM and EDS volumes separately and the combined HAADF-EDS HEBT [17] method will be compared. The impact of the number of

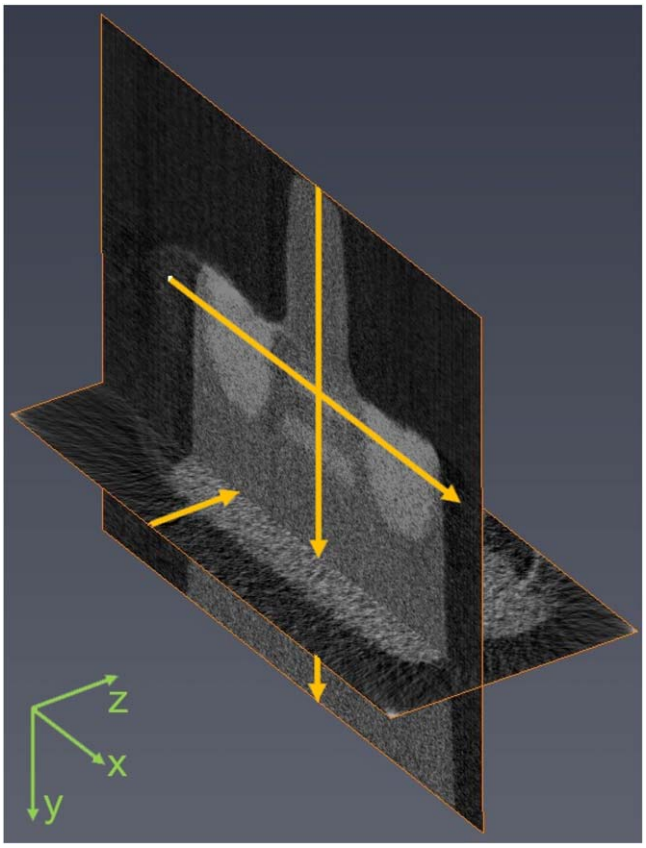

Figure 4. Orthoslices across the reconstructed volume with indication of the positions of the line scans used to investigate the reconstruction quality. The slices shown in the picture correspond with the HEBT 100 iterations $\alpha = 0.6$ HAADF reconstruction. Identical positions are used for all analyzed conditions.

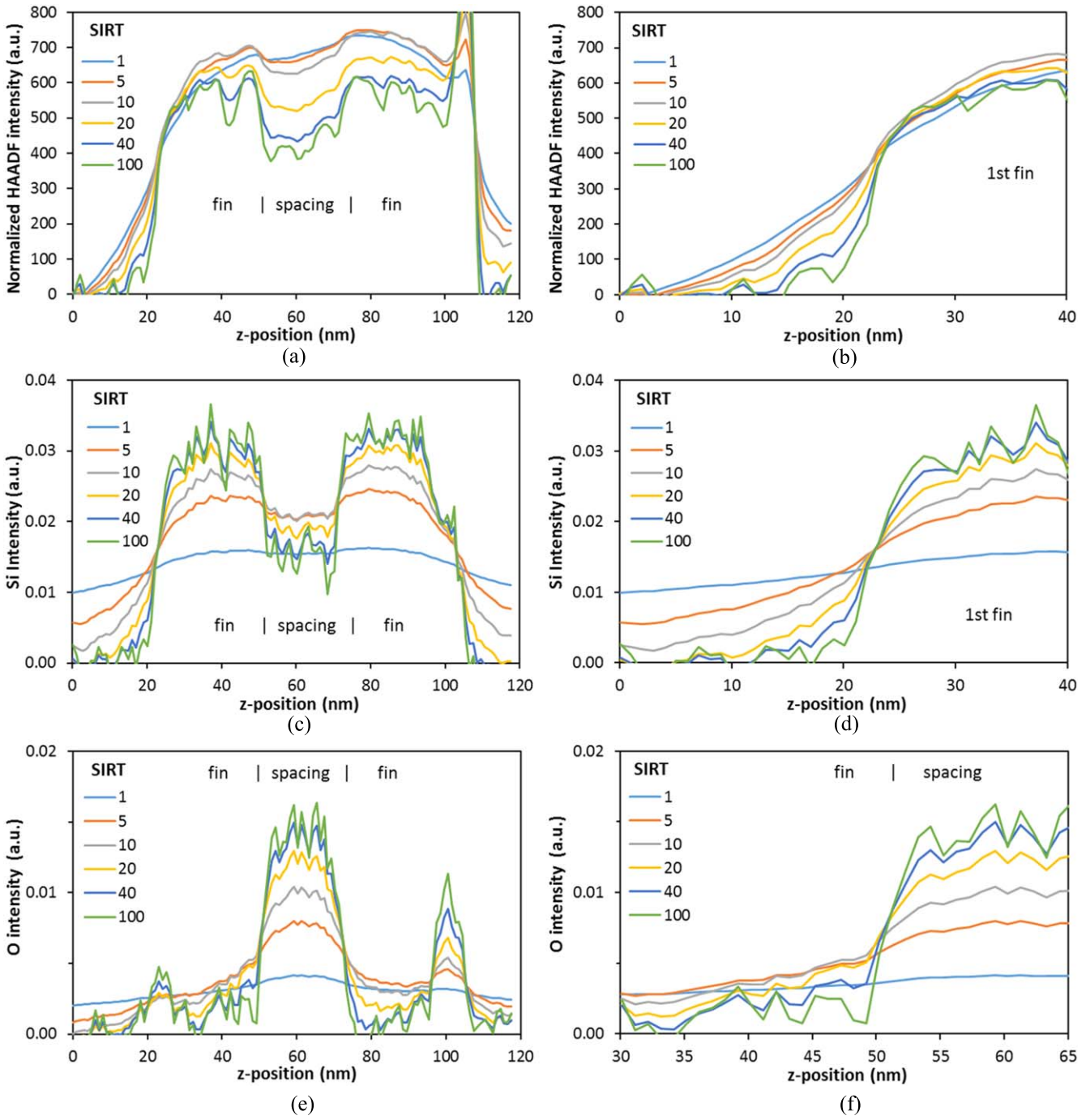

Figure 5. Intensity profiles in *z*-direction across the bulk fins through the SIRT reconstructed volume at the position marked on figure 4 for HAADF (normalized at the origin, (a), (b)), Si (c), (d) and O (e), (f). The right graphs are zooms at the left interface of the 1st fin (b, d) and at the interface with the STI oxide spacing (f). *yz*-slices at this position are shown on supplementary figure S2 is available online at stacks.iop.org/SST/34/114002/mmedia.

iterations, HEBT weighting factor and filtering of the EDS data on the reconstruction quality will be analyzed from an application point of view.

Experiments

The investigated structures are partially processed wafers taken from an experimental process flow for devices with vertically stacked Si nanowires (NW) and gate-all-around replacement metal gate (GAA-RMG) [23–25]. The structure consists of Si/SiGe multilayered fins covered by poly-crystalline Si dummy gates and with the processing finished by the epitaxial growth of recessed Si-liner/SiGe source/drains (S/D).

For the tomography sample preparation, the structure is covered by a spin-on-carbon (SOC) layer and ion beam deposited Pt in the FIB. The pillar samples are mounted on W

wires centered on 1 mm Cu shafts (GGB Industries) which fit in the Fischione 2050 on-axis rotation tomography holder. Instead of the classically used conical-cylindrically shaped pillars, rectangular pillars are used. It allows a much faster preparation based on the methods applied for standard plane-parallel TEM specimens combined with lateral milling steps. The region of interest remains clear in the SEM image during this lateral milling and hence the pillar can accurately be centered on the feature of interest. The method is illustrated on figure 1 for a fin/gate device structure. For the gate and fin dimensions of the investigated structures, a volume containing S/D, one gate and 3 fins corresponds to pillars with a nearly square shaped cross-section (270 nm edges) while pillars with only 2 fins included have a rectangular cross-section ($\sim 270 \times 120$ nm^2).

Acquisition of combined STEM/EDS tomography series is done with the TomoSTEM-Velox software. A 120 keV beam energy is used with convergence angle 7.8 mrad in a double corrected Titan^3 G2 60–300 microscope which allows a 180° tilt range of the stage. The series are obtained from −90° to +90° in steps of 2° or 3° acquiring simultaneously ABF/DF/HAADF and EDS maps (764 × 860 pixels) at each step. The EDS acquisition is done with a SuperX detector integrating for 300 s and netcounts maps are saved in mrc-files for the relevant elements, i.e. for the x-ray lines Si K, Ge L, O K and N K. Alignment of the series and 3D reconstructions are performed with Inspect3D version 4.3. The alignment is done with cross-correlation on the HAADF-STEM series and applied to the EDS series as well. Reconstructions are performed with the SIRT and HEBT methods as available in the software. To evaluate the quality of the reconstruction results, line scans are extracted across the volume with Avizo 9.4 software. For the calculation of S/N, lines with single voxel diameter are used, while for the determination of contrast between the materials and of the spatial resolution at interfaces, an averaging over a volume with 4 nm radius is applied. The spatial resolution is defined as the interface width between 16 and 84% of the signal.

Results

A schematic of the investigated structure and HAADF-STEM images of the pillar sample oriented nearly along the <110> directions of the Si substrate are shown on figure 2. In this case, the sample volume contains 2 fins, 1 gate and the full S/D regions. The two <110> directions correspond with viewing along the gate and along the fins respectively. The SOC is almost completely etched during the O_2/Ar plasma clean applied before the tomography acquisition. Therefore, the Pt cap became unstable and is tilted (anyhow not of interest).

The standard STEM images (figures 2(b), (c)) can be used to benchmark the subsequent tomography acquisition and reconstruction quality. The nitride spacer shows almost no contrast on HAADF-STEM versus the poly-Si gate. More contrast is however observed on DF-STEM or TEM images. The SiGe of the S/D has diamond shapes and these are well

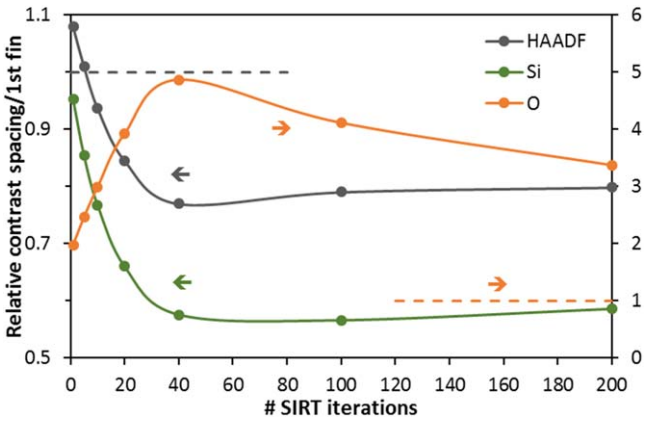

Figure 6. Relative contrast in the STI oxide spacing versus the first fin for the HAADF, Si and O SIRT reconstructed volumes as determined for the z-line scan across the bulk fins indicated on figure 4. The dashed lines correspond to no-contrast. The O-data refer to the right axis.

separated between the fins. In the image parallel to the fin the SiGe in the S/D is therefore thicker in projection, hence the higher brightness compared to the SiGe wires under the gate should not be interpreted as a composition difference. The shallow trench isolation oxide (STI)/poly-Si gate interface is situated near the bottom of the lowest SiGe wire. The oxide is however irregularly deeper etched between the S/D. As these recesses were filled with SOC, they correspond to voids in the final sample after the plasma etch. As can be expected after 30 keV FIB, the outer surfaces of the Si are amorphized over a thickness ∼25 nm. It can also be noticed that on one side of the pillar redeposition of Pt-particles occurred during the FIB preparation.

SIRT

SIRT reconstruction [14] is applied to the HAADF and EDS tilt series with the alignment of the series performed on the STEM images. The reconstructions themselves are however independent. Slices parallel to the fins reconstructed with 40 SIRT iterations are shown in figure 3. The two slice positions are selected in the center of the first fin and in the center of the STI spacing between the fins respectively. On the first set of slices, weak contrast can be observed between the substrate and the bulk fin on both the HAADF and the Si map, and oxygen signal is present in the bulk fin. As substrate and bulk fin are pure Si, these observations give indication that the spatial resolution in the z direction is worse than half the width of the bulk fin, i.e. worse than $\sim 22/2 = 11$ nm. Similar conclusion can be derived for the second slice position where based on the standard imaging conditions (figure 2(c)) no bright HAADF contrast or Ge signal are expected between the S/D regions. The bottom of the gate in the STI spacing between the fins is obvious on the Si and O slices (figure 3(b)) but can hardly be recognized from the HAADF slice. The nitride spacer shows no clear contrast on the HAADF reconstruction and is also not clear on the Si slices while it is obvious on the N-slices which show that the pillar volume also includes the spacers of the next gates. These free-standing spacers however became unstable during the imaging

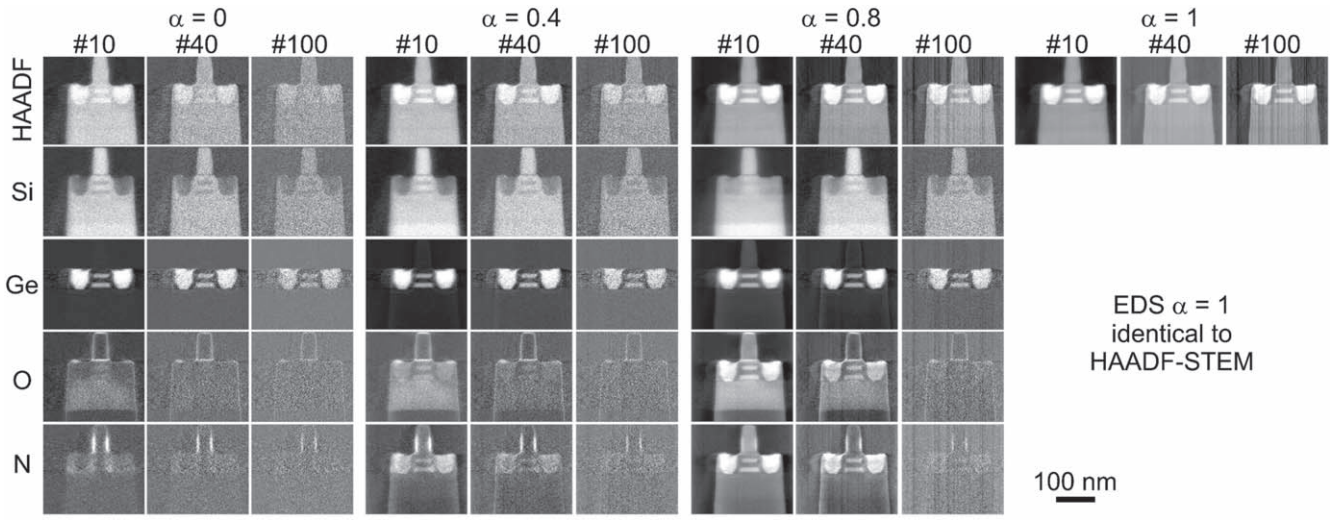

Figure 7. Tableau of *xy* slices parallel the first fin for HAADF, Si K, Ge L, O K and N K as function of the number of HEBT iterations (10, 40, 200) and for weight factors 0 (a), 0.4 (b), 0.8 (c) and 1 (d). All images are scaled to the range of the brightness histogram. The *y*-line scans indicated on figure 4 lie in these slices.

and fell over in the empty spaces above the S/D. All these observations illustrate the benefits of combined HAADF/EDS tomography to reach full interpretation of the morphology and composition of the structures.

Line scans along critical positions in the volume are used to extract quantitative data on spatial resolution and materials contrasts. The positions of these lines along x, y and z directions are illustrated on figure 4 and are kept constant for all analyzed conditions. Line scans in z-direction across the bulk fins are shown on figure 5 as function of the number of SIRT iterations for the HAADF, Si and O reconstructions. The HAADF intensities are normalized at the origin of the graphs. The steep rise of the intensity near 100 nm is due to the Pt redeposition layer at that side of the pillar. On front and back side of the pillar only some thin oxide is present, i.e. the pillar milling stopped on both sides just before the bulk fins. For all signals the interface width as measured between the bending points of the profiles decreases with the number of iterations from ∼20 nm (5 iterations) to ∼4–5 nm (100 iterations). Even from 40 to 100 iterations a minor improvement can still be noticed but further increase to 200 iterations (not shown) has no effect anymore on the interface widths. The relative contrast between the materials as defined by the ratio of the signals above the minimum is shown on figure 6 comparing the STI spacing (SiO_2) and the first bulk fin (Si). It reaches a maximum for about 40 iterations. Further increasing the number of SIRT iterations results in decreasing contrast which is caused by an increase of the noise. Ideally the relative signal ratio should reflect the compositional ratio, i.e. the square ratio of the average atomic number Z for the HAADF and the atomic density ratios for the EDS. Taking into account the material densities yields $Z^2_{SiO2}/Z^2_{Si} \sim 0.73$, and the atomic density ratios are 0.44 for Si and infinite for O as oxygen should in principle be absent in the fin. Considering that x-ray absorption effects are not considered [9, 18] and that, due to the limited spatial z-resolution, the O signal is not fully absent in the bulk fins, the experimental values are roughly in accordance with these expectations. Hence after ∼40 iterations the contrasts in the slices are a fair measure for the local composition.

HEBT

The bimodal HEBT reconstruction method [17] links the HAADF-STEM images and the different EDS maps through the calculation of 'response ratio factors', which are computed as the coefficients of a linear regression, assuming that each HAADF projection is a linear combination of the corresponding elemental maps at the same tilt. The low intensity EDS maps are scaled with respect to the HAADF maps. The HEBT method then reconstructs the elemental maps by simultaneously minimizing the residuals for each element separately as well as the residual of the linear combination of the elements compared to the HAADF projections. The relative importance of these two contributions is adjusted by a weighting factor α. The extreme case $\alpha = 0$ corresponds per-element to the application of the standard SIRT routine to the elemental maps, while the HAADF-STEM reconstruction yields in that case a combination of all EDS maps. On the other hand, for $\alpha = 1$ the HAADF as well as all EDS reconstructions yield the standard SIRT reconstruction of the HAADF only.

The HEBT reconstruction is applied to the dataset for the weighting factor α varying from 0 to 1 in steps of 0.2 and for the number of iterations in the range 1–400. Figure 7 shows a tableau of xy slices through the first bulk fin as a function of the weighting factor α and the number of iterations. Due to the link with the noisy EDS maps, all STEM slices are noisier than the SIRT result which corresponds to the $\alpha = 1$ case. For $\alpha = 0$ the HAADF-STEM data are not considered and the HAADF-STEM reconstruction therefore yields a combination of the EDS signals. It is noisy and shows a poor contrast

between different materials. Hence for the HAADF-STEM images the standard SIRT reconstruction is the better choice.

The EDS maps show an improvement of the contrast for increasing α. For small number of iterations a shadow effect of the STEM image can be seen as is obvious for the 10 and 40 iteration cases for the O and N maps which show a high intensity in the regions corresponding to the bright, i.e. Ge-rich, areas on the HAADF-STEM image. Also, on the Ge slice with 10 iterations a shadow of the Si-gate and bulk fin/substrate can be noticed. However, all these effects diminish for high number of iterations. Qualitatively it can be concluded that a HEBT reconstruction requires both a high number of iterations and a quite high weighting factor. This is in line with the results obtained for the phantom objects and Au–Ag particles [17].

The impact of α and the number of iterations on the noise and contrast is further evaluated based on line scans extracted at the same position as discussed for the SIRT reconstruction as well as on line scans vertically along the y direction through the center of the first fin (positions marked on figure 4). The line scans across the bulk fins (figure 8) show that the z-resolution improves for increasing number of iterations and becomes for high number of iterations independent of the weighting factor. For a small number of iterations (20–40) the spatial resolution improves for decreasing α factor and is the best for $\alpha = 0$ which corresponds for the EDS data to application of the standard SIRT reconstruction. For the STEM data the weighting factor has almost no effect on the spatial resolution at the interface.

The relative contrast between the STI oxide spacing and the first bulk fin is analyzed on figure 9. The best contrast is obtained for high number of iterations and large weighting factor α, e.g. for Si 200 iterations, $\alpha = 0.6$ or 400 iterations, $\alpha = 0.8$, and for O 100 iterations, $\alpha = 0.6$ or 200 iterations, $\alpha = 0.8$. In both cases the contrast is better than with standard SIRT due to a contribution to the contrast induced by the correlation with the HAADF signal. On the other hand, the standard SIRT gives the best HAADF contrast and this already after 40 iterations.

The O line scans in y-direction across the first bulk fin (position indicated on figure 4, the xy slices are given in figure 7) show oxygen signal in the bulk fin in the reconstruction with 40 iterations for all weight factors while the oxygen level is strongly reduced for higher number of iterations (figures 10(a), (b)). For high weighting factor α the link with the HAADF can lead to an overshoot of the EDS signal due to the high brightness regions in the STEM images. This effect is obvious for the $\alpha = 0.8$ curve on figure 10(a) where 2 strong peaks appear at the position of the SiGe wires. From the line scans the contrast relative to the substrate is calculated in the bulk fin and in the thin SiO_2 gate oxide layer between fin and gate. In the bulk fin ideally no O is detected, i.e. only noise should be present similar as in the substrate and the relative contrast should be equal to 1. Such condition can be reached for 100 iterations with $\alpha = 0$ (equivalent to standard SIRT) and requires a further increasing number of iterations as the weighting factor increases (figure 10(c)). On the other hand, in the gate oxide a high relative contrast is desirable which can be reached for small number of iterations or, combined with better spatial resolution, for higher number of iterations and high α (figure 10(d)). Hence the requirements for best z-resolution (low α) and high contrast in the oxide layer (high α) are opposite and a compromise must be made.

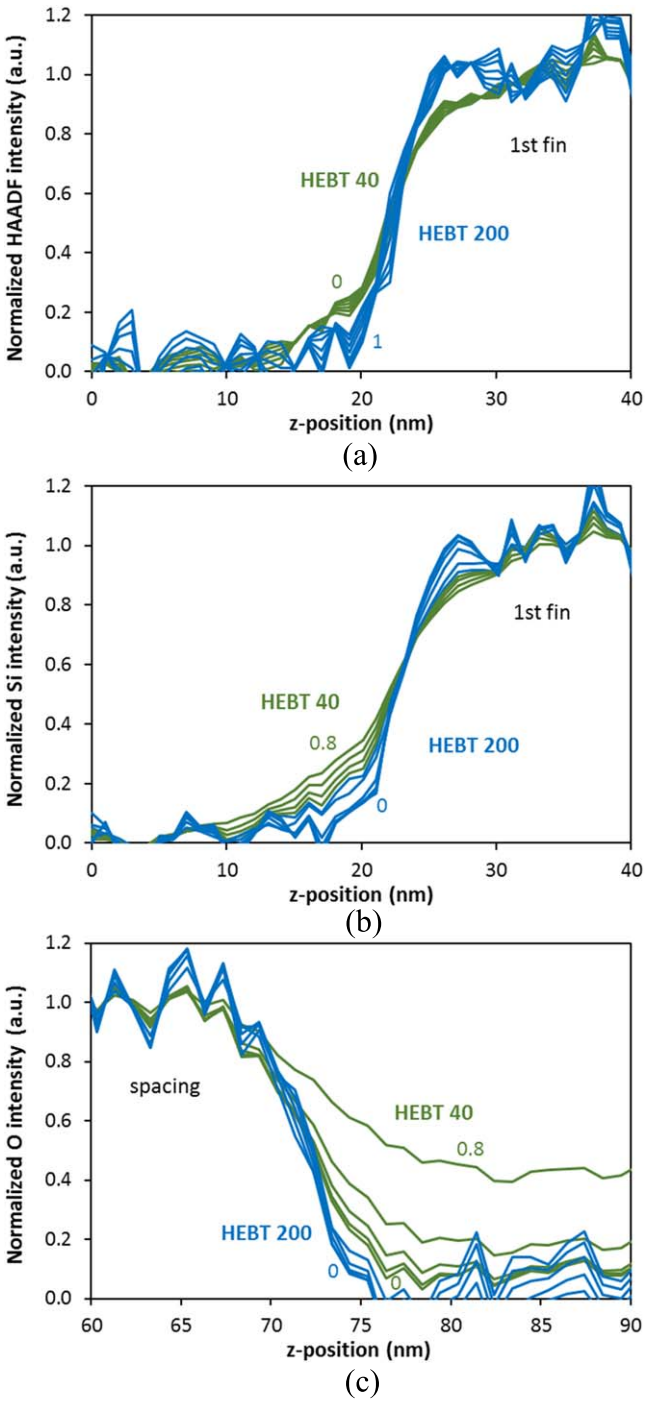

Figure 8. Intensity profiles in z-direction across the bulk fins through the HEBT reconstructed volume at the same position as used for figure 5: HAADF (a), Si (b) and O (c). The curves are normalized for comparison of the interfacial resolution. For each bundle the upper curve corresponds to weight factor 0 in (a) and to 0.8 in (b), (c), while the lowest curves correspond to weight factor 1 and 0 respectively.

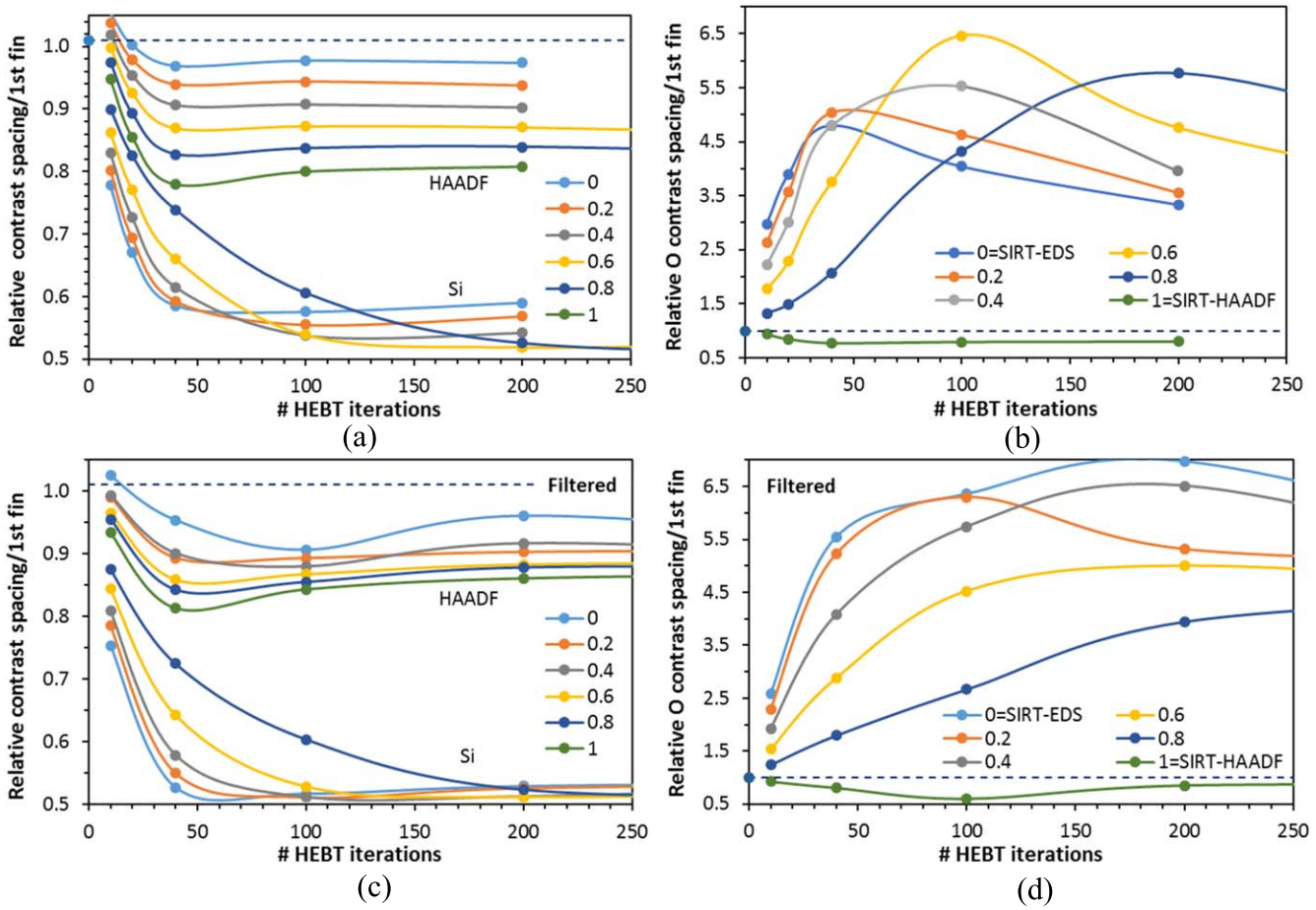

Figure 9. Relative contrast in the STI spacing versus the first fin for the HAADF, Si and O HEBT reconstructed volumes as a function of the number of iterations and for the weighting factor in the range 0–1 without (a), (b) and with (c), (d) Gaussian filtering of the EDS data. The dashed lines correspond to no-contrast.

Noise

As can be noticed qualitatively on the images of figures 3 and 7 and the different line scans, the noise in the reconstructed slices increases with the number of iterations. The relative standard deviation is taken as a measure for the noise in the reconstructions. It is determined for the relevant elements of the different materials in a fixed length of the *y*-line scan indicated on figure 4, i.e. in the slices corresponding to figure 7. In all cases the noise initially decreases strongly and reaches a minimum at 20 iterations (figure 11). For SIRT EDS the minimum is reached already after 10 iterations. With SIRT, the HAADF shows only a weak increase of the noise for further increasing number of iterations while for HEBT the noise increases steeply for all signals up to 100 iterations and shows a weaker dependence for further increased number of iterations. Increasing α results in a decrease of the noise which is obviously due to the growing importance of the contribution of the less noisy HAADF signal. The reduction of the noise by the iteration procedure is generally considered as a major advantage of SIRT over the simpler weighted backprojection [2] with an optimum reached after 20–30 iterations [20].

Reduction of the noise in the EDS data can also be obtained by filtering prior to the reconstruction [7]. A despeckle and Gaussian filter is applied in Avizo to the original EDS data and HEBT reconstruction is applied similar as for the unfiltered data. Depending on the number of iterations, it results in a reduction of the relative standard deviations while retaining the resolution (supplementary figure S5). Particularly for the small number of iterations it improves the contrast between the materials (figures 9(c), (d)).

Spatial resolution

The spatial resolution is determined for the relevant signals at different interfaces of the line scans indicated on figure 4, i.e. at the outer bulk fin interface (Si, *z*-direction), the STI interface (O, *z*-direction), top Ge layer (Ge, *y*-direction) and SiGe S/D (Ge, *x*-direction). At all positions also the spatial resolution for the HAADF-STEM reconstructions is measured. A summary of the results is represented in figure 12. The general trend for all conditions shows an improvement of the spatial resolution up to 40 iterations for SIRT and even 100 iterations for HEBT. The resolution for *x* and *z* directions are similar as can be expected based on the pillar shape configuration of the sample and the 180° tilt range. The resolution in *y*-direction shows, except for the very first iteration, no dependence on the number of iterations, i.e. it is determined

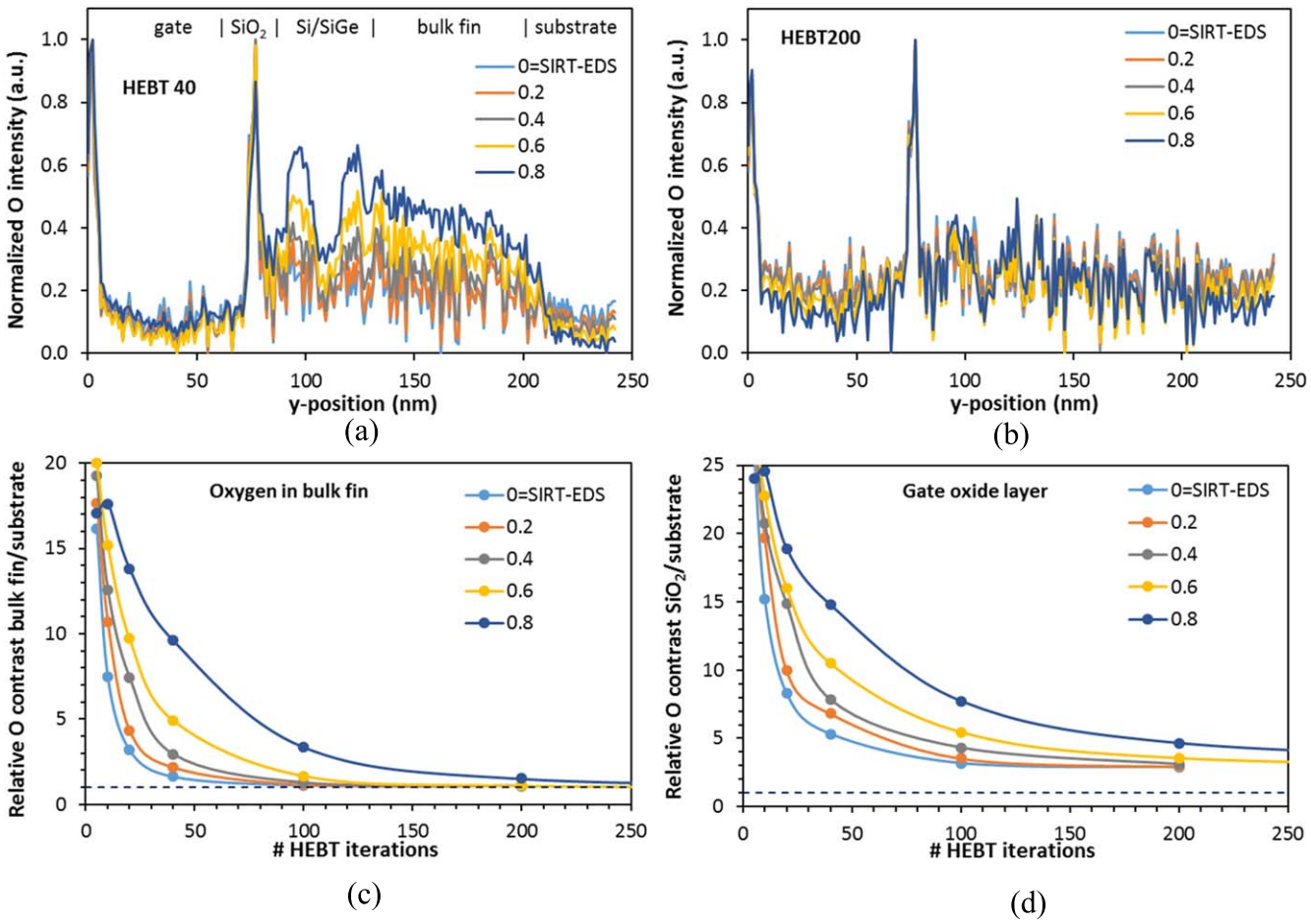

Figure 10. Normalized O line profiles along *y*-direction across the center of the first bulk fin for 40 (a) and 200 (b) HEBT iterations and α from 0 to 0.8, and contrast of the O signal in the bulk fin (c) and in the gate oxide (d) relative to the substrate. The line scan position is indicated on figure 4.

by the resolution in the images and x-ray maps. For SIRT reconstruction the spatial resolution for STEM and EDS maps are similar which is not the case for HEBT. The resolution for HAADF with HEBT is worse than for SIRT, which is due to the higher noise and weaker contrast. For EDS the HEBT-resolution only weakly depends on the weighting factor for α in the range 0–0.6 but degrades for higher α. This is particularly the case for the O signal for which due to the increasing influence of the HAADF-STEM contrast, the onset of a contrast reversal occurs for high weighting factors which degrades the spatial resolution (supplementary information figure S5). Except for this latter case, the spatial resolution in all directions converges to ~5 nm.

An estimate of the expected spatial resolution d can be made from the Crowther formulae [19] under the assumption of perfectly aligned tomographic series with a $+90°$ to $-90°$ tilt range:

$$d_x = d_z = \pi D/N$$

with D the diameter of the reconstructed volume and N the number of tilt steps. For the applied conditions this yields a resolution of ~13 nm which is much worse than the experimentally obtained results which show that by applying a sufficiently high number of iterations, a ~2.5 times better spatial resolution is possible. This agrees with the work of Mezerji *et al* [20] who also obtained a two times better resolution for STEM reconstructions when applying 10–20 SIRT iterations. The faster saturation of the resolution with the number of iterations in that work is likely related to the smaller volume and hence higher magnifications used for the tomography acquisition.

The spatial resolution $d_{\mathrm{tomo-EDS}}$ for EDS tomography with filtered backprojection is estimated as [5]:

$$d_{\mathrm{tomo-EDS}} = \sqrt{2}\, d_{\mathrm{EDS}}$$

with d_{EDS} the 2D analytical spatial resolution which is limited by the noise in the EDS maps and beam broadening in thicker specimens. For the conditions used for this analysis d_{EDS} will be on the order of 2–3 nm, hence the experimental tomographic resolution agrees well with this formula.

The experimental resolutions are affected by the fact that the analysis is not done on smooth and sharp interfaces, i.e. the roughness of the considered interfaces and the fact that the line scans are not always perfectly orthogonal to the interfaces will result in worse resolution than ideally possible. Hence the obtained results represent a practical resolution for the considered device but can nevertheless be expected to be relevant for similar sized volumes. For analysis of device structures

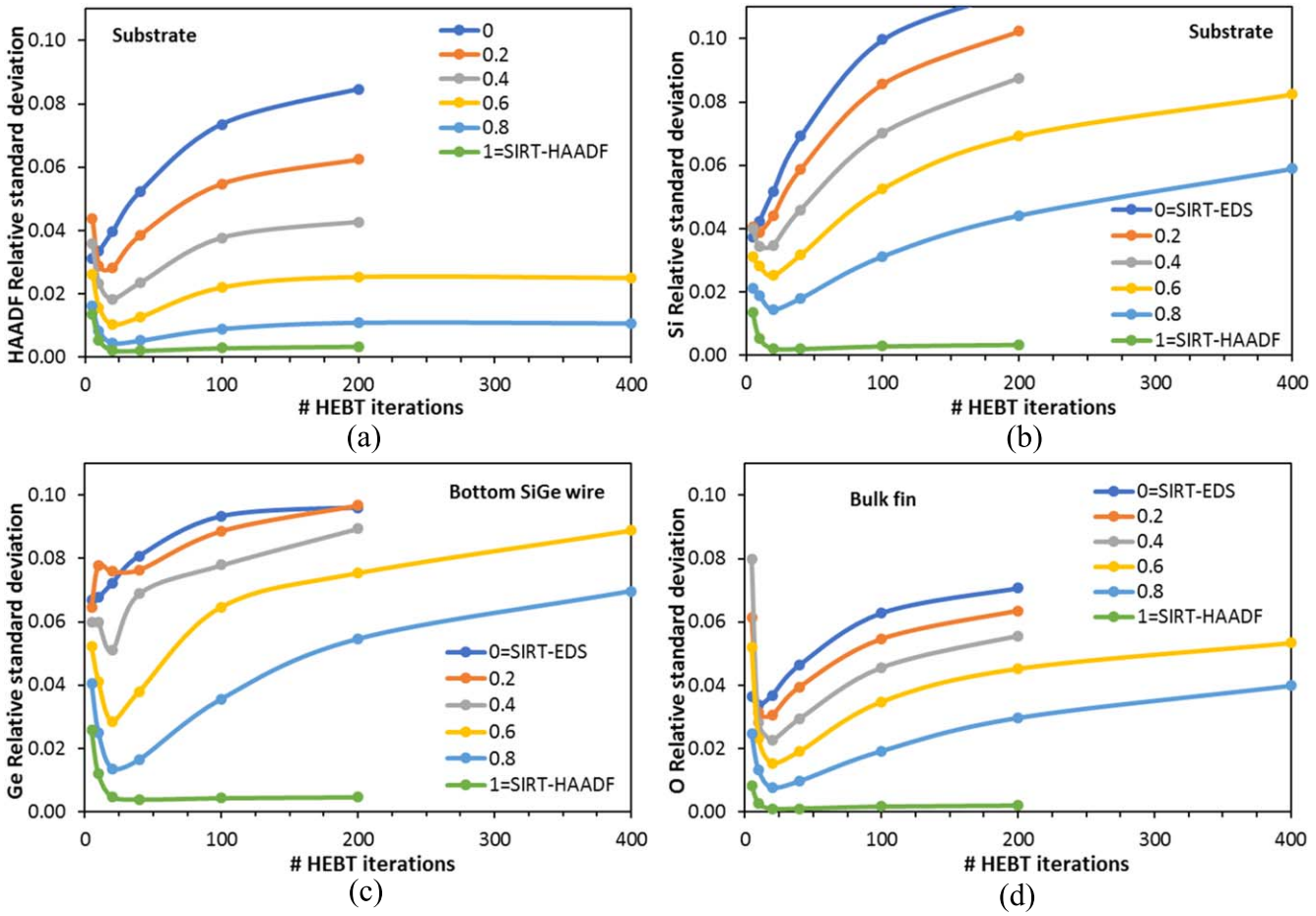

Figure 11. Evolution of the noise in the reconstruction with number of iterations and weighting factor α as determined in the *xy* slice across the first bulk fin: in the substrate for HAADF (a) and Si K (b), in the bottom wire for Ge L (c) and in the bulk fin for O K (d).

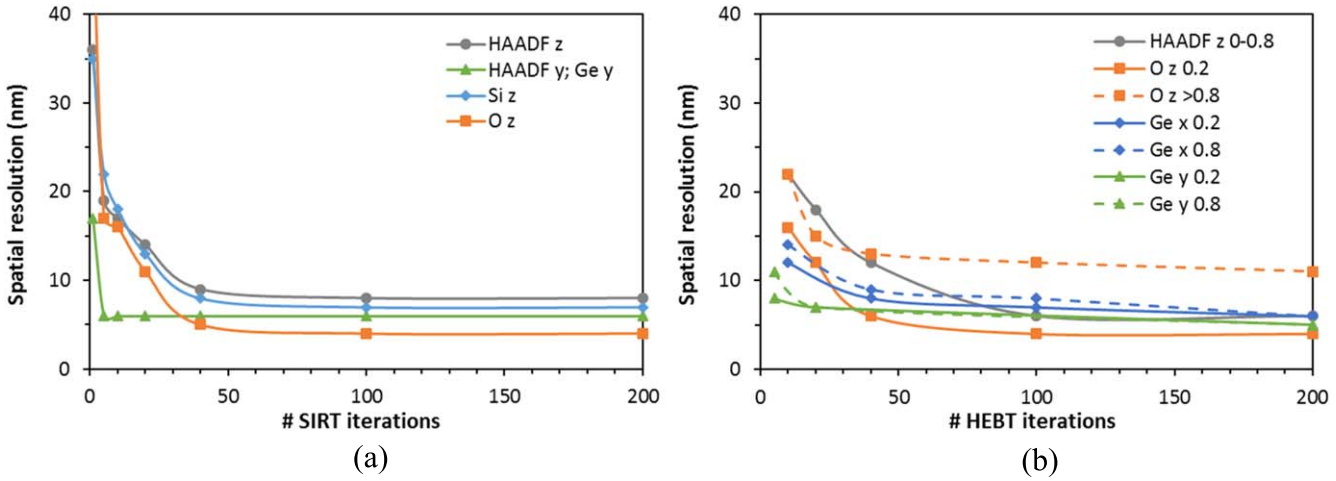

Figure 12. Spatial resolution as measurement on different interfaces of the line scans shown in figure 4 as function of the number of iterations for SIRT (a) and HEBT (b) reconstruction for the indicated signals and direction. For the HEBT reconstructions results.

with a volume as considered in this work, options to further improve the spatial resolution would be to increase the number of tilt steps which would lead, even with the most advanced EDS detectors, to unrealistic data acquisition times. On the other hand, future further scaling of the device structures may allow to reduce the analyzed volume which will also result in improvement of the spatial resolution. Employing algorithms that consider prior knowledge about the sample might also help to improve the reconstructions and spatial resolution.

Conclusions

The reconstruction quality of a $+/-90^{\circ}$ tilt series is analyzed for a pillar shaped sample with rectangular cross-section including a partially processed 3D transistor structure. Both standard SIRT applied to the STEM images and EDS maps separately and the HEBT method which combines all data sets are considered.

The spatial resolution at the interfaces between different materials improves up to 40 (SIRT) or 100 (HEBT) iterations. The best spatial resolution obtained for the investigated dataset is on the order on 4–5 nm and is similar for both STEM and EDS. A high number of iterations results in all cases in increased noise in the reconstructions, which can however be reduced by increasing the weighting factor in the HEBT algorithm. Alternatively, the noise can also be reduced by filtering the raw EDS data before the reconstruction. Whereas the contrast between different materials initially increases with the number of iterations, the increase of the noise degrades the contrast for too high number of iterations. Increasing α improves contrast but leads for $\alpha > 0.8$ to unwanted ghost contrast in the EDS slices and degradation of the spatial resolution due to increasing importance of the contribution to the contrast originating from the HAADF signal. In practice one must make a compromise between best resolution (i.e. high number of iterations and $\alpha < 0.8$) and optimum contrast/not too high noise (i.e. medium number of iterations and high α).

For higher number of iterations, the brightness in the SIRT reconstructed slices is a rough measure for the compositions but for accurate quantification also absorption effects in the relatively thick pillars should be considered. However, in the HEBT case, for increasing α the brightness is affected by the brightness of the HAADF-image and therefore the direct relation with composition gets lost.

The present results can be used as guidelines for combined STEM-EDS tomography analysis of advanced 3D nanodevices. Further improvement of the spatial resolution will be possible for further scaled devices which will allow to reduce the pillar diameter while still including a full functional device in its volume.

Acknowledgments

The research is supported by the program 'Automated multimodal tomography for sub-22 nm IC nodes' (project 13314) of the Netherlands Organization for Scientific Research (NWO) and by the Electronic Component Systems for European Leadership Joint Undertaking under grant agreement 692527.

Patricia Van Marcke is acknowledged for the FIB preparation and Hans Mertens and the imec processing groups for providing the research material.

ORCID iDs

Hugo Bender https://orcid.org/0000-0003-0209-2597
Paromita Kundu https://orcid.org/0000-0003-2526-8372
Paola Favia https://orcid.org/0000-0002-1019-3497
Willem Jan Palenstijn https://orcid.org/0000-0003-0511-4763
Holger Kohr https://orcid.org/0000-0003-0727-9561

References

[1] Kuhn K J 2012 Considerations for ultimate CMOS scaling *Trans. Electron Devices* **59** 1813–28
[2] Kubel C, Voigt A, Schoenmakers R, Otten M, Su D, Lee T-C, Carlsson A, Engelmann H-J and Bradley J 2005 Recent advances in electron tomography: TEM and HAADF-STEM tomography for materials science and IC applications *Microsc. Microanal.* **11** 378–400
[3] Ercius P, Weyland M, Muller D A and Gignac L M 2006 Three-dimensional imaging of nanovoids in copper interconnects using incoherent bright field tomography *Appl. Phys. Lett.* **88** 243116
[4] Bender H, Richard O, Kalio A and Sourty E 2007 3D-analysis of semiconductor structures by electron tomography *Microelectron. Eng.* **84** 2707–13
[5] Möbus G, Doole R C and Inkson B J 2003 Spectroscopic electron tomography *Ultramicroscopy* **96** 433–51
[6] Genc A, Kovarik L, Gu M, Cheng H, Plachinda P, Pullan L, Freitag B and Wang C 2013 XEDS STEM tomography for 3D chemical characterization of nanoscale particles *Ultramicroscopy* **131** 24–32
[7] Lepinay K, Lorut F, Pantel R and Epicier T 2013 Chemical 3D tomography of 28 nm high K metal gate transistor: STEM XEDS experimental method and results *Micron* **47** 43–9
[8] Goris B, Polavarapu L, Bals S, Van Tendeloo G and Liz-Marzán L M 2014 Monitoring galvanic replacement through three-dimensional morphological and chemical mapping *Nano Lett.* **14** 3220–6
[9] Burdet P, Saghi Z, Filippin A N, Borrás A and Midgley P A 2016 A novel 3D absorption correction method for quantitative EDX-STEM tomography *Ultramicroscopy* **160** 118–29
[10] Slater T J A, Janssen A, Camargo P H C, Burke M G, Zaluzec N J and Haigh S J 2016 STEM-EDX tomography of bimetallic nanoparticles: a methodological investigation *Ultramicroscopy* **162** 61–73
[11] Fu B and Gribelyuk M A 2018 3D analysis of semiconductor devices: a combination of 3D imaging and 3D elemental analysis *J. Appl. Phys.* **123** 161554
[12] Goris B, Roelandts T, Batenburg K J, Mezerji H H and Bals S 2013 Advanced reconstruction algorithms for electron tomography: from comparison to combination *Ultramicroscopy* **127** 40–7
[13] Collins S M and Midgley P A 2017 Progress and opportunities in EELS and EDS tomography *Ultramicroscopy* **180** 133–41
[14] Gilbert P 1972 Iterative methods for the three-dimensional reconstruction of an object from projections *J. Theor. Biol.* **36** 105–17
[15] Guo Y, Aveyard R and Rieger B 2019 A multichannel cross-modal fusion framework for electron tomography *IEEE Trans. Image Process.* **28** 4206–18
[16] Saghi Z, Xu X, Peng Y, Inkson B and Möbus G 2007 Three-dimensional chemical analysis of tungsten probes by energy dispersive x-ray nanotomography *Appl. Phys. Lett.* **91** 251906
[17] Zhong Z, Goris B, Schoenmakers R, Bals S and Batenburg K J 2017 A bimodal tomographic reconstruction technique combining EDS-STEM and HAADF-STEM *Ultramicroscopy* **174** 35–45

[18] Bender H, Seidel F, Favia P, Richard O and Vandervorst W 2017 X-ray absorption in pillar shaped transmission electron microscopy specimens *Ultramicroscopy* **177** 58–68
[19] Crowther R A, de Rosier D J and Klug A 1970 The reconstruction of a three-dimensional structure from projections and its application to electron microscopy *Proc. R. Soc.* A **317** 319–40
[20] Mezerji H H, Van den Broek W and Bals S 2011 A practical method to determine the effective resolution in incoherent experimental electron tomography *Ultramicroscopy* **111** 330–6
[21] Arslan I, Yates T J V, Browning N D and Midgley P A 2005 Embedded nanostructures revealed in three dimensions *Science* **309** 2195–8
[22] Van Aert S, Batenburg K J, Rossell M D, Erni R and Van Tendeloo G 2011 Three-dimensional atomic imaging of crystalline nanoparticles *Nature* **470** 374–7
[23] Mertens H *et al* 2016 Gate-all-around MOSFETs based on vertically stacked horizontal Si nanowires in a replacement metal gate process on bulk Si substrates *VLSI Tech. Dig.* pp 158–9
[24] Mertens H *et al* 2016 Vertically stacked gate-all-around Si nanowire CMOS transistors with dual work function metal gates *IEDM Tech. Dig.* pp 524–7
[25] Favia P *et al* 2019 TEM investigations of gate-all-around nanowire devices *Semicond. Sci. Technol.* (in press) (https://doi.org/10.1088/1361-6641/ab4b8b)